Covert Underwater Communications with Multiband OFDM

Geert Leus*, Paul van Walree†, Jeroen Boschma†, Claudio Fanciullacci‡, Hans Gerritsen§ and Paolo Tusoni¶
*Delft University of Technology, Mekelweg 4, 2628 CD Delft, The Netherlands; g.j.t.leus@tudelft.nl
†TNO, Oude Waalsdorperweg 63, 2509 JG The Hague, The Netherlands; {paul.vanwalree, jeroen.boschma}@tno.nl
‡Teleport Eutelsat, Route de Cerquese, 78660 Prunay-en-Yvelines, France; cfanciullacci@eutelsat.fr
§Moog FCS, Pesetaweg 53, 2153 PJ Nieuw Vennep, The Netherlands; jvwgerritsen@chello.nl
¶Value Team, Via della Grande Muraglia 284, 00144 Rome, Italy; paolo.tusoni@valueteam.com

***Abstract*— We consider the use of orthogonal frequency division multiplexing (OFDM) for covert acoustic telemetry. To reduce the complexity of the receiver we use a multiband approach, modulating each band by OFDM. The system has been tested at sea in a highly time-varying environment. A total bandwidth of 3.6 kHz was divided in 16 subbands. Data rates of 4.2 and 78 bit/s were adopted over ranges up to 52 km. At 78 bit/s, communication is successful at SNRs down to -8 dB, whereas the lower rate allows data transfer at SNRs down to at least -16 dB.**

I. Introduction

We study covert communications in an acoustic underwater environment. In this paper, covert means that data can be decoded at a low signal-to-noise ratio (SNR), thereby hiding the signal in the ambient noise and decreasing the risk of detection by third parties. Auditive aspects are also important, which favors noiselike waveforms based on phase-shift keying (PSK) over, for instance, chirp-based modulations. Direct-sequence spread spectrum is a possible candidate to meet the objective [1], [2], but we show in this paper that orthogonal frequency division multiplexing (OFDM) is a strong contender. The study was carried out in the frame of the joint European research project UUV Covert Acoustic Communications (UCAC), which aims at the establishment of a covert acoustic link between unmanned underwater vehicles (UUVs) and a distant mother platform.

The use of OFDM in underwater communications is not new, see for example [3]–[5]. However, compared to these works, this paper contains a number of novel contributions:

- The long delay spread encountered in littoral areas requires a long OFDM symbol duration in order to limit the redundancy of the cyclic prefix. However, this may result in a considerable channel time variability within a single OFDM symbol, causing a loss of orthogonality among the carriers. We deal with this problem by modeling and estimating the channel within an OFDM symbol as a basis expansion model (BEM). In [3]–[5], much simpler channel models have been considered, which are no longer valid for large Doppler spreads and/or long OFDM symbols.
- The long OFDM symbol duration will also result in a large number of carriers, which makes the above channel estimation procedure rather complex. To reduce this complexity we consider a multiband OFDM approach, where the available frequency band is divided into smaller subbands, each of which is modulated by OFDM.
- We aim at covert communications and thus we rely on coding and spreading operations to allow for a low bit error rate (BER) at a low signal to noise ratio (SNR).

Let us now describe our proposed transceiver in some more detail. At the transmitter, we start by broadcasting a template that will be used for acquisition and synchronization. Then, the information bits are turbo encoded and modulated. The resulting data symbol stream is further parsed into OFDM symbols that are also imprinted with some specific pilot design used for channel estimation. Every OFDM symbol is finally spread over different time slots and frequency bands.

At the receiver, we first run an acquisition and synchronization procedure. The receiver correlates the received signal with a bank of different Doppler shifted versions of the acquisition template. As soon as the correlator output exceeds some threshold, the signal is acquired and a time and frequency offset are available. The signal is corrected for these offsets and we can proceed to recover the information bits. First, we exploit the pilot design to estimate the channel in every OFDM symbol. To capture the possible channel time variability, we model and estimate the channel within a single OFDM symbol as a BEM. Based on the obtained channel estimates, we subsequently perform a low-complexity joint equalization and despreading procedure to extract every information-carrying OFDM symbol. Finally, turbo decoding is carried out to recover the information bits.

Notation: We use upper (lower) case bold face letters to denote matrices (column vectors). $(\cdot)^*$, $(\cdot)^T$, $(\cdot)^H$, and $(\cdot)^\dagger$, represent conjugate, transpose, complex conjugate transpose (Hermitian), and pseudo inverse (Moore-Penrose inverse), respectively. $\lfloor x \rfloor$ and $\lceil x \rceil$ round x toward the nearest integer smaller than or equal to x and larger than or equal to x, respectively, $\Re(x)$ denotes the real part of x, and $\mathrm{E}(\cdot)$ stands for the expectation. a mod b gives the remainder of a divided by b. $\mathrm{diag}(\mathbf{x})$ stands for a diagonal matrix with $\mathbf{x}$ as diagonal, and $\mathrm{diag}(\mathbf{X}_0, \ldots, \mathbf{X}_{N-1})$ for the block diagonal matrix with $\mathbf{X}_0, \ldots, \mathbf{X}_{N-1}$ as diagonal blocks. We use $[\mathbf{x}]_n$ to indicate the n-th element of $\mathbf{x}$ (counting from 0), and $[\mathbf{X}]_{n,m}$ to

978-1-4244-2620-1/08/$25.00 ©2008 IEEE

indicate the (n,m)-th entry of $\mathbf{X}$ (counting from 0). Further, $[\mathbf{x}]_{n:n'}$ indicates the subvector of $\mathbf{x}$ from element n to n' (counting from 0) and $[\mathbf{X}]_{n:n',m:m'}$ indicates the submatrix of $\mathbf{X}$ from row n to n' and from column m to m' (counting from 0), where only the colon is kept when all rows or columns are included (Matlab notation). Next, $\mathbf{I}_N$ denotes the $N \times N$ identity matrix and $\mathbf{0}_{M\times N}$ the $M \times N$ all-zero matrix. Finally, $\mathbf{F}_N$ stands for the unitary N-point DFT matrix with $[\mathbf{F}_N]_{n,m} = \frac{1}{\sqrt{N}} \mathrm{e}^{-\iota \frac{2\pi}{N} nm}$, where we define $\iota = \sqrt{-1}$.

II. Data Model

Before we can set up a communications link, we need to run an acquisition and synchronization procedure. Since this is not the core of the current paper, we only describe this briefly. We start by sending a template consisting of a maximal-length sequence modulated on sinc pulses. At the receiver, the hydrophone signal is correlated with a bank of different Doppler shifted versions of the transmitted template. Next, the peak filter output is obtained across all Doppler branches, and as soon as it crosses a certain threshold the signal is considered acquired with corresponding delay and Doppler shifts. Following detection, the template is stripped off and the remaining signal is delay-Doppler shifted, such that the strongest multipath arrival is centered in the causal impulse response representing the acoustic channel.

For the subsequent developments, we move to a digital bandpass data model at rate $1/T$, much larger than the signal bandwidth. This rate $1/T$ could for instance be the rate required for the transmitter, or the digitization rate at the receiver. Transitions to and from another rate can easily be incorporated by means of a resampling operation. The data model we adopt is

$$\bar{v}[n] = \sum_{l=0}^{L_h-1} \bar{h}[n;l]\bar{u}[n-l] + \bar{\varepsilon}[n], \tag{1}$$

where $\bar{u}[n]$ is the transmitted signal, $\bar{v}[n]$ is the received signal, $\bar{\varepsilon}[n]$ represents the additive noise, and $\bar{h}[n;l]$ models the remaining acoustic channel as a causal time-varying finite impulse response (FIR) filter with length L_h and with a centered chief multipath arrival. Notice that although such a model is generally adopted for narrowband systems, it also holds for wideband systems because the time variation of the FIR filter can capture this wideband nature. Other time-varying effects that can be modeled by $\bar{h}[n;l]$ are transmitter and receiver motion as well as the reflections off moving scatterers or the moving sea surface.

The data model (1) is the starting point of our multiband OFDM approach. For ease of presentation, we assume in the following sections that the acquisition and synchronization steps have already been carried out and that the data transmission can start at time instant $n = 0$.

III. Transmitter

Fig. 1 depicts the overall transmitter structure, while Fig. 2 details the subband processing block of Fig. 1. A bit sequence is first turbo encoded and modulated onto a PSK alphabet. The resulting data symbols are then parsed into blocks of length K_d. Each block of K_d data symbols is interleaved with K_t training symbols (pilots), leading to a sequence of $K\times 1$ ($K = K_\mathrm{d} + K_\mathrm{t}$) vectors $\mathbf{s}_p$, $p = 0, 1, \ldots, P-1$, which we assume to have energy K. We will come back to the specific pilot design later on. These $K \times 1$ vectors $\mathbf{s}_p$ will now be spread out over J subbands with I OFDM symbols each. Denoting the i-th OFDM symbol of the j-th subband by the $K \times 1$ vector $\mathbf{s}_i^{(j)}$, with $i = 0, 1, \ldots, I-1$ and $j = 0, 1, \ldots, J-1$, we will assume that $\mathbf{s}_p$ is spread out over the set $\{\mathbf{s}_i^{(j)}\}$ with indices $(i,j) \in \mathcal{I}_p$, i.e., $\mathbf{s}_i^{(j)} = \mathbf{s}_p$ if $(i,j) \in \mathcal{I}_p$.

Every $K \times 1$ OFDM symbol $\mathbf{s}_i^{(j)}$ is transformed into an $N \times 1$ baseband time domain vector $\mathbf{x}_i^{(j)}$ with samples at a rate of $1/T$. This can be done by inserting $N-K$ zeros in the middle of $\mathbf{s}_i^{(j)}$ and transforming the result by means of an N-point unitary IDFT:

$$\mathbf{x}_i^{(j)} = \mathbf{F}_N^H \mathbf{T} \mathbf{s}_i^{(j)}, \tag{2}$$

where $\mathbf{T}$ is the $N \times K$ zero inserting matrix given by $\mathbf{T} = [[\mathbf{I}_{K/2}, \mathbf{0}_{K/2\times K/2}]^T, \mathbf{0}_{K,N-K}, [\mathbf{0}_{K/2\times K/2}, \mathbf{I}_{K/2}]^T]^T$. Note that this operation can actually be interpreted as transforming $\mathbf{s}_i^{(j)}$ by means of a K-point unitary IDFT, then upsampling it with a factor N/K, and finally circularly lowpass filtering it with a unit-energy filter.

In the next step, a cyclic prefix (CP) of N_cp samples is added, which results in the $(N + N_\mathrm{cp}) \times 1$ vector $\mathbf{u}_i^{(j)} = [[\mathbf{x}_i^{(j)}]_{N-N_\mathrm{cp}:N-1}^T, \mathbf{x}_i^{(j)T}]^T$. The reason for this CP is that it simplifies the equalization process, since if the channel (including all delay effects) fits within the CP, the channel in (1) resembles a quasi-circular convolution at the receiver[1], and a single input vector will be related to only one output vector.

OFDM waveforms normally have a high peak-to-average power ratio (PAPR). The use of identical pilots in every vector, and the simultaneous occurrence of two or more identical vectors $\mathbf{s}_p$ in two or more subbands, further increases the PAPR. This limits the power output of the employed transducers, which is not a major drawback in the context of covertness, but which limits the maximum range. To contain the PAPR of the compound waveform, the last two operations on $\mathbf{u}_i^{(j)}$, which we rewrite for convenience as $\mathbf{u}_i^{(j)} = [u_i^{(j)}[0], \ldots, u_i^{(j)}[N + N_\mathrm{cp} - 1]]^T$, insert a timing offset of N_j samples to reduce the PAPR, and modulate the signal onto a carrier of frequency f_j, chosen such that the subbands will not overlap. These operations lead to the following contribution of the i-th OFDM symbol of the j-th subband to the transmitted signal $\bar{u}[n]$:

$$\bar{u}_i^{(j)}[n] = \begin{cases} \sqrt{\dfrac{2E}{KN}} \Re[u_i^{(j)}(n - n_i^{(j)}) \exp(\iota 2\pi f_j n T)], \\ \qquad \text{if } n = n_i^{(j)}, \ldots, n_i^{(j)} + N + N_\mathrm{cp} - 1 \\ 0, \qquad \text{otherwise} \end{cases}, \tag{3}$$

[1]We use the term "quasi-circular" for the generalization of the term "circular" to time-varying filters.

where $n_i^{(j)} = N_j + i(N+N_{\rm cp})$ and E/T is the average power per subband. The overall transmitted sequence can then be written as

$$\bar{u}[n] = \sum_{i=0}^{I-1} \sum_{j=0}^{J-1} \bar{u}_i^{(j)}[n], \tag{4}$$

with an average power of JE/T. This sequence is finally applied at the input of the transmitter.

IV. Receiver

As mentioned, we assume that acquisition and synchronization have been carried out as indicated in Section II, allowing us to adopt the data model (1). We then carry out the reverse of the steps that were taken at the transmitter, followed by channel estimation, equalization and despreading, and turbo decoding. The overall receiver structure is illustrated in Fig. 3, with Fig. 4 detailing the operations carried out in each subband.

In order to recover the i-th OFDM symbol of the jth subband, we first select the correct $N + N_{\rm cp}$ samples from $\bar{v}[n]$, taking into account the timing offset of N_j samples, and remove the carrier f_j. In other words, we construct the following signal:

$$v_i^{(j)}[n-n_i^{(j)}] = \begin{cases} \sqrt{\dfrac{2KN}{E}}\bar{v}[n]\exp(-\iota 2\pi f_j nT), \\ \quad \text{if } n = n_i^{(j)}, \ldots, n_i^{(j)} + N + N_{\rm cp} - 1 \\ 0, \quad \text{otherwise} \end{cases}, \tag{5}$$

where we normalize the output power with respect to the input power. We implicitly assume that an ideal lowpass filtering is carried out at this point in order to remove the double frequencies and reach an equivalent baseband representation. Next the CP is stripped from the $(N + N_{\rm cp}) \times 1$ vector $\mathbf{v}_i^{(j)} = [v_i^{(j)}[0], \ldots, v_i^{(j)}[N + N_{\rm cp} - 1]]^T$, which is reduced to the $N \times 1$ vector $\mathbf{y}_i^{(j)} = [\mathbf{v}_i^{(j)}]_{N_{\rm cp}:N+N_{\rm cp}-1}$.

On the assumption that i) the CP length $N_{\rm cp}$ is large enough for the channel to fit within the CP for every subband, i.e., $N_{\rm cp} \geq L_h - 1 + \max_{j,j'}(N_j - N_{j'})$, ii) the subband carriers f_j are separated by $(K+G)/(NT)$, where $1/(NT)$ is the carrier spacing and $G/(NT)$ is some frequency guard between the subbands, and iii) the guard $G/(NT)$ is larger than the maximal Doppler spread, then $\mathbf{y}_i^{(j)}$ only depends on the i-th OFDM symbol of the j-th subband if the K carriers of interest are chosen. Hence, the multiband interference can be completely removed by transforming the $N \times 1$ baseband time-domain vector $\mathbf{y}_i^{(j)}$ by means of an N-point unitary DFT and selecting from it the first $K/2$ and last $K/2$ carriers, which leads to the $K \times 1$ vector $\mathbf{z}_i^{(j)}$:

$$\begin{aligned} \mathbf{z}_i^{(j)} &= \mathbf{T}^T \mathbf{F}_N \mathbf{y}_i^{(j)} \\ &= \mathbf{T}^T \mathbf{F}_N (\mathbf{H}_i^{(j)} \mathbf{x}_i^{(j)} + \boldsymbol{\zeta}_i^{(j)}), \end{aligned} \tag{6}$$

where $\boldsymbol{\zeta}_i^{(j)}$ is similarly defined from $\bar{\varepsilon}[n]$ as $\mathbf{y}_i^{(j)}$ from $\bar{v}[n]$, and where $\mathbf{H}_i^{(j)}$ is the $N \times N$ quasi-circular channel matrix of interest given by $[\mathbf{H}_i^{(j)}]_{n,n'} = h_i^{(j)}[n; (n-n') \bmod N]$ with $h_i^{(j)}[n;l] = \bar{h}[n_i^{(j)} + N_{\rm cp} + n; l]\exp(-\iota 2\pi f_j l T)$.

Similar to (2), it can be shown that (6) can be interpreted as first circularly lowpass filtering $\mathbf{y}_i^{(j)}$ with a unit-energy filter, then downsampling it by a factor N/K, and finally transforming it by means of a K-point unitary DFT.

These alternative interpretations for (2) and (6) allow us to relate $\mathbf{z}_i^{(j)}$ to $\mathbf{s}_i^{(j)}$ as

$$\begin{aligned} \mathbf{z}_i^{(j)} &= \mathbf{T}^T \mathbf{F}_N \mathbf{H}_i^{(j)} \mathbf{F}_N^H \mathbf{T} \mathbf{s}_i^{(j)} + \boldsymbol{\eta}_i^{(j)} \\ &= \mathbf{F}_K \boldsymbol{\Lambda}_i^{(j)} \mathbf{F}_K^H \mathbf{s}_i^{(j)} + \boldsymbol{\eta}_i^{(j)}, \end{aligned} \tag{7}$$

where $\boldsymbol{\eta}_i^{(j)}$ is similarly defined from $\boldsymbol{\zeta}_i^{(j)}$ as $\mathbf{z}_i^{(j)}$ from $\mathbf{y}_i^{(j)}$, and $\boldsymbol{\Lambda}_i^{(j)}$ is the $K \times K$ quasi-circular channel matrix given by $[\boldsymbol{\Lambda}_i^{(j)}]_{k,k'} = \lambda_i^{(j)}[k; (k-k') \bmod K]$ with $\lambda_i^{(j)}[k;l]$ the N/K-times downsampled version of a left and right unit-energy lowpass filtered version of $h_i^{(j)}[n;l]$. Using frequency-domain matrices, we obtain

$$\begin{aligned} \mathbf{z}_i^{(j)} &= \mathbf{T}^T \tilde{\mathbf{H}}_i^{(j)} \mathbf{T} \mathbf{s}_i^{(j)} + \boldsymbol{\eta}_i^{(j)} \\ &= \tilde{\boldsymbol{\Lambda}}_i^{(j)} \mathbf{s}_i^{(j)} + \boldsymbol{\eta}_i^{(j)}, \end{aligned} \tag{8}$$

where $\tilde{\mathbf{H}}_i^{(j)} = \mathbf{F}_K \mathbf{H}_i^{(j)} \mathbf{F}_K^H$ and $\tilde{\boldsymbol{\Lambda}}_i^{(j)} = \mathbf{F}_K \boldsymbol{\Lambda}_i^{(j)} \mathbf{F}_K^H$. Note that the smoothness of $h_i^{(j)}[n;l]$, which leads to a circularly banded frequency domain channel matrix $\tilde{\mathbf{H}}_i^{(j)}$, carries over to the smoothness of $\lambda_i^{(j)}[k;l]$, leading to a circularly banded frequency domain channel matrix $\tilde{\boldsymbol{\Lambda}}_i^{(j)}$. This is also clear from (8), where we can see that $\tilde{\boldsymbol{\Lambda}}_i^{(j)}$ simply is a submatrix of $\tilde{\mathbf{H}}_i^{(j)}$. Hence, if $\tilde{\mathbf{H}}_i^{(j)}$ has a bandwidth B, then $\tilde{\boldsymbol{\Lambda}}_i^{(j)}$ has a bandwidth B. Notice that this bandwidth even reduces to $B = 1$ in the time-invariant case. In that case $\tilde{\mathbf{H}}_i^{(j)}$ and $\tilde{\boldsymbol{\Lambda}}_i^{(j)}$ are diagonal, with the frequency response of $h_i^{(j)}[n;l]$ and $\lambda_i^{(j)}[k;l]$ on the diagonal, respectively.

A. Channel Estimation

In this section, an algorithm is proposed that estimates the acoustic underwater channel for individual OFDM symbols. In other words, only the pilots inside $\mathbf{s}_i^{(j)}$ will be used to estimate $\tilde{\boldsymbol{\Lambda}}_i^{(j)}$. To this end we exploit the structure that is present in $\tilde{\boldsymbol{\Lambda}}_i^{(j)}$, or equivalently the structure that is present in $\boldsymbol{\Lambda}_i^{(j)}$. Ignoring for simplicity the temporal sidelobes of the lowpass filtering of $h_i^{(j)}[n;l]$, we may assume that $\lambda_i^{(j)}[k;l]$ is a causal time-varying FIR filter with length $L_\lambda = \lceil (L_h - 1)K/N \rceil + 1$. Furthermore, the smoothness of every tap $\lambda_i^{(j)}[k;l]$ can be exploited by means of a so-called basis expansion model (BEM) [6], [7]. More specifically, we will model $\boldsymbol{\lambda}_i^{(j)}[l] = [\lambda_i^{(j)}[0;l], \ldots, \lambda_i^{(j)}[K-1;l]]^T$ as a superposition of Q fixed functions $\mathbf{b}_q = [b_q[0], \ldots, b_q[K-1]]^T$ weighted with Q channel-dependent coefficients $c_{i,q}^{(j)}[l]$, with $Q \ll K$:

$$\boldsymbol{\lambda}_i^{(j)}[l] = \sum_{q=0}^{Q-1} \mathbf{b}_q c_{i,q}^{(j)}[l] = \mathbf{B}\mathbf{c}_i^{(j)}[l], \tag{9}$$

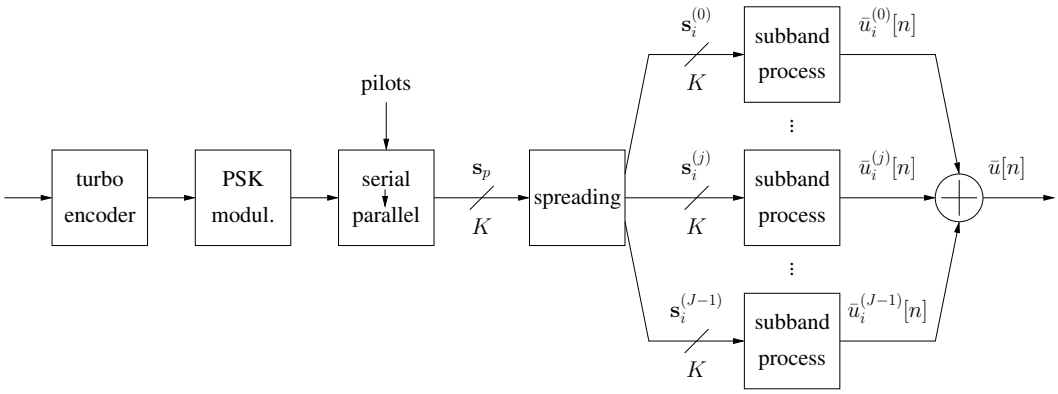

Fig. 1. Block diagram of the transmitter operations.

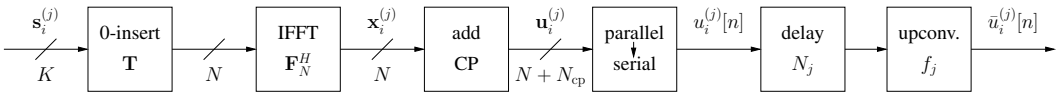

Fig. 2. Block diagram of the subband processing at the transmitter.

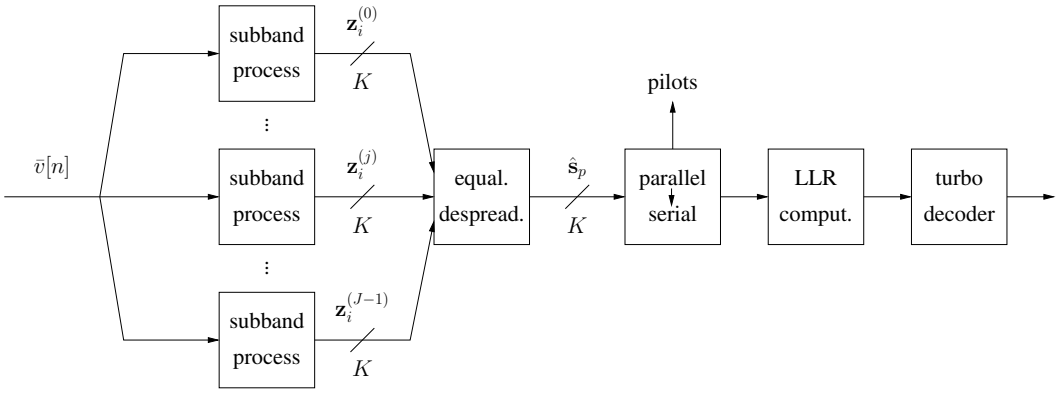

Fig. 3. Block diagram of the receiver operations.

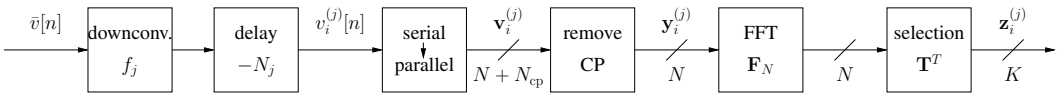

Fig. 4. Block diagram of the subband processing at the receiver.

where $\mathbf{B} = [\mathbf{b}_0, \ldots, \mathbf{b}_{Q-1}]$ is the BEM functions matrix and $\mathbf{c}_i^{(j)}[l] = [c_{i,0}^{(j)}[l], \ldots, c_{i,Q-1}^{(j)}[l]]^T$ is the BEM coefficient vector related to the l-th tap. In this manner the number of unknowns for the l-th tap is reduced from K to Q.

To estimate the BEM coefficients, we use the K_{t} training symbols (pilots) that were inserted in every block of K_{d} data symbols as discussed in Section III. The pilot scheme we consider here is the one proposed in [7], where every $\mathbf{s}_p$ (and thus every OFDM symbol $\mathbf{s}_i^{(j)}$) consists of M pilot clusters of length K_{t}/M. For the m-th pilot cluster, denoted as $\check{\mathbf{s}}_m = [\mathbf{s}_i^{(j)}]_{k_m:k_m+K_{\text{t}}/M-1}$, we then select a related set of received samples $\check{\mathbf{z}}_{i,m}^{(j)} = [\mathbf{z}_i^{(j)}]_{k_m+D:k_m+K_{\text{t}}/M-D-1}$, where D is a parameter that can be used to control the number of output samples that are selected. Referring to [7] for more details, it is then possible to express $\check{\mathbf{z}}_i^{(j)} = [\check{\mathbf{z}}_{i,0}^{(j)T}, \ldots, \check{\mathbf{z}}_{i,M-1}^{(j)T}]^T$ as

$$\check{\mathbf{z}}_i^{(j)} = \check{\mathbf{S}}\mathbf{c}_i^{(j)} + \check{\mathbf{d}}_i^{(j)}, \tag{10}$$

where $\mathbf{c}_i^{(j)} = [\mathbf{c}_{i,0}^{(j)T}, \ldots, \mathbf{c}_{i,Q-1}^{(j)T}]^T$ with $\mathbf{c}_{i,q}^{(j)} = [c_{i,q}^{(j)}[0], \ldots, c_{i,q}^{(j)}[L_\lambda - 1]]^T$, where $\check{\mathbf{S}}$ depends on $\check{\mathbf{s}}$, and where $\check{\mathbf{d}}_i^{(j)}$ is some interference term.

In [7], different methods have been proposed to solve (10) for $\mathbf{c}_i^{(j)}$, which is complicated by the fact that the inference term $\check{\mathbf{d}}_i^{(j)}$ itself depends on $\mathbf{c}_i^{(j)}$. For simplicity reasons, we

apply the least-squares estimator in this work:

$$\hat{\mathbf{c}}_i^{(j)} = \check{\mathbf{S}}^{\dagger}\check{\mathbf{z}}_i^{(j)}. \tag{11}$$

For more complex estimators, such as the best linear unbiased estimator or the linear minimum mean square error (LMMSE) estimator, we refer the interested reader to [7]. An estimate for $\tilde{\mathbf{\Lambda}}_i^{(j)}$ can now easily be constructed using (9) and the relation between $\tilde{\mathbf{\Lambda}}_i^{(j)}$ and $\mathbf{\Lambda}_i^{(j)}$.

Note that the channel estimation complexity is $\mathcal{O}(KL_\lambda^2Q^2)$ per OFDM symbol, or in total $\mathcal{O}(IJKL_\lambda^2Q^2)$. For a single band of JK carriers the complexity is $\mathcal{O}\left(IJKJ^2L_\lambda^2Q^2\right) = \mathcal{O}\left(IJ^3KL_\lambda^2Q^2\right)$, since the channel length increases by a factor J. Hence, the multiband OFDM approach significantly reduces the channel estimation complexity compared to traditional OFDM.

B. Equalization and Despreading

In this section dealing with equalization and despreading, we assume that every OFDM symbol $\mathbf{s}_i^{(j)}$ or $\mathbf{s}_p$, which was assumed to have energy K, is white with unit variance:

$$\mathrm{E}\left(\mathbf{s}_i^{(j)}\mathbf{s}_i^{(j)H}\right) = \mathrm{E}\left(\mathbf{s}_p\mathbf{s}_p^H\right) = \mathbf{I}_K, \tag{12}$$

and that the different noise vectors $\boldsymbol{\eta}_i^{(j)}$ are white and mutually uncorrelated with different variances:

$$\mathrm{E}\left(\boldsymbol{\eta}_i^{(j)}\boldsymbol{\eta}_{i'}^{(j')H}\right) = \begin{cases} \sigma_i^{(j)2}\mathbf{I}_K, & \text{if } i = i' \text{ and } j = j' \\ \mathbf{0}_{K\times K}, & \text{otherwise} \end{cases}. \tag{13}$$

The variances $\sigma_i^{(j)2}$ are estimated with the help of null subcarriers in the pilot clusters (see Section V).

Instead of following a suboptimal two-step approach consisting of equalization followed by despreading, we here propose a joint approach with improved results. To derive the joint approach, we start by stacking all the output vectors related to the same input vector, $\mathbf{z}_p = [\ldots, \mathbf{z}_i^{(j)T}, \ldots]^T,\ (i,j) \in \mathcal{I}_p$, leading to

$$\mathbf{z}_p = \tilde{\mathbf{\Lambda}}_p\mathbf{s}_p + \boldsymbol{\eta}_p, \tag{14}$$

where $\boldsymbol{\eta}_p$ is similarly defined as $\mathbf{z}_p$ and $\tilde{\mathbf{\Lambda}}_p = [\ldots, \tilde{\mathbf{\Lambda}}_i^{(j)T}, \ldots]^T,\ (i,j) \in \mathcal{I}_p$. Owing to the assumption (13), the covariance matrix of $\boldsymbol{\eta}_p$ is given by $\mathbf{R}_p = \mathrm{E}(\boldsymbol{\eta}_p\boldsymbol{\eta}_p^H) = \mathrm{diag}(\ldots, \sigma_i^{(j)2}\mathbf{I}_K, \ldots),\ (i,j) \in \mathcal{I}_p$. From (14), we can then estimate $\mathbf{s}_p$ by linear processing. Adopting an LMMSE estimator, we obtain

$$\begin{aligned}
\hat{\mathbf{s}}_p &= \hat{\tilde{\mathbf{\Lambda}}}_p^H(\hat{\tilde{\mathbf{\Lambda}}}_p\hat{\tilde{\mathbf{\Lambda}}}_p^H + \hat{\mathbf{R}}_p)^{-1}\mathbf{z}_p \\
&= (\hat{\tilde{\mathbf{\Lambda}}}_p^H\hat{\mathbf{R}}_p^{-1}\hat{\tilde{\mathbf{\Lambda}}}_p + \mathbf{I}_K)^{-1}\hat{\tilde{\mathbf{\Lambda}}}_p^H\hat{\mathbf{R}}_p^{-1}\mathbf{z}_p \\
&= \left(\sum_{(i,j)\in\mathcal{I}_p} \hat{\sigma}_i^{(j)-2}\hat{\tilde{\mathbf{\Lambda}}}_i^{(j)H}\hat{\tilde{\mathbf{\Lambda}}}_i^{(j)} + \mathbf{I}_K\right)^{-1} \\
&\qquad \times \sum_{(i,j)\in\mathcal{I}_p} \hat{\sigma}_i^{(j)-2}\hat{\tilde{\mathbf{\Lambda}}}_i^{(j)H}\mathbf{z}_i^{(j)},
\end{aligned} \tag{15}$$

where $\hat{\tilde{\mathbf{\Lambda}}}_p$, $\hat{\tilde{\mathbf{\Lambda}}}_i^{(j)}$, $\hat{\mathbf{R}}_p$, and $\hat{\sigma}_i^{(j)}$ represent the estimated versions of $\tilde{\mathbf{\Lambda}}_p$, $\tilde{\mathbf{\Lambda}}_i^{(j)}$, $\mathbf{R}_p$, and $\sigma_i^{(j)}$.

Note that the complexity of the joint equalization and despreading operation is $\mathcal{O}(K^3)$ per data symbol vector, or in total $\mathcal{O}(PK^3)$. For a single band of JK carriers this complexity is $\mathcal{O}(P/JJ^3K^3) = \mathcal{O}(PJ^2K^3)$, since the number of data symbol vectors decreases by a factor J. Hence, the multiband OFDM approach also significantly reduces the complexity of the joint equalization and despreading operation compared to traditional OFDM. However, this is not true when the circularly banded nature of $\tilde{\mathbf{\Lambda}}_i^{(j)}$ is taken into account [8]–[11]. Remember that $\tilde{\mathbf{\Lambda}}_i^{(j)}$ can be assumed to have a bandwidth B, which in the time-invariant case reduces to $B = 1$ when $\tilde{\mathbf{\Lambda}}_i^{(j)}$ is diagonal. For this case, the complexity of the joint equalization and despreading operation is reduced to $\mathcal{O}(KB^2)$ per data symbol vector, or in total $\mathcal{O}(PKB^2)$, which equals the complexity of a single band with JK carriers.

C. Turbo Decoding

A standard turbo decoder is used to decode the encoded bits [12]. At the input it requires the log-likelihood ratios (LLRs) of the encoded bits after equalization, and the output consists of the estimated information bits before encoding. The question that remains is how we compute the a priori LLRs of the encoded bits after equalization. To do this, we first have to derive the probability density function (PDF) of the estimated data symbols $s_p[k] = [\mathbf{s}_p]_k$ given that the related transmitted data symbol was α. The exact derivation of this conditional PDF is involved, but we may approximate it as Gaussian with mean $\mu_{p,\alpha}[k]$ and variance $\sigma_{p,\alpha}^2[k]$, a common procedure in turbo equalization [13]. Specifically, the mean $\mu_{p,\alpha}[k]$ and variance $\sigma_{p,\alpha}^2[k]$ can be derived from [13] as

$$\mu_{p,\alpha}[k] = t_p[k]\alpha \tag{16}$$

$$\sigma_{p,\alpha}^2[k] = t_p[k]\left(1 - t_p[k]\right), \tag{17}$$

where

$$\begin{aligned}
t_p[k] &= [\hat{\tilde{\mathbf{\Lambda}}}_p^H\left(\hat{\tilde{\mathbf{\Lambda}}}_p\hat{\tilde{\mathbf{\Lambda}}}_p^H + \hat{\mathbf{R}}_p\right)^{-1}\hat{\tilde{\mathbf{\Lambda}}}_p]_{k,k} \\
&= [(\hat{\tilde{\mathbf{\Lambda}}}_p^H\hat{\mathbf{R}}_p^{-1}\hat{\tilde{\mathbf{\Lambda}}}_p + \mathbf{I}_K)^{-1}\hat{\tilde{\mathbf{\Lambda}}}_p^H\hat{\mathbf{R}}_p^{-1}\hat{\tilde{\mathbf{\Lambda}}}_p]_{k,k} \\
&= \left[\left(\sum_{(i,j)\in\mathcal{I}_p} \hat{\sigma}_i^{(j)-2}\hat{\tilde{\mathbf{\Lambda}}}_i^{(j)H}\hat{\tilde{\mathbf{\Lambda}}}_i^{(j)} + \mathbf{I}_K\right)^{-1}\right. \\
&\qquad \left.\times \sum_{(i,j)\in\mathcal{I}_p} \hat{\sigma}_i^{(j)-2}\hat{\tilde{\mathbf{\Lambda}}}_i^{(j)H}\hat{\tilde{\mathbf{\Lambda}}}_i^{(j)}\right]_{k,k}.
\end{aligned} \tag{18}$$

Using these formulations for $\mu_{p,\alpha}[k]$ and $\sigma_{p,\alpha}^2[k]$, one can compute the LLRs of the encoded bits after equalization for different PSK alphabets as indicated in [13].

Note that channel estimation, equalization and despreading, as well as turbo decoding can also run in an iterative loop, where in each step the performance is improved, similar to [13]–[16]. However, owing to complexity reasons we do not consider such an iterative framework for the proposed acoustic communication system.

V. EXPERIMENTS

The multiband OFDM system described above has been tested during sea trials in northern Europe in August/September 2007. The objective was to set up a communications link over long distances in a covert manner. The available bandwidth was 3.6 kHz. The preamble template consisted of a maximal-length sequence of length 4095 modulated on sinc pulses with a bandwidth of 3.6 kHz at a rate of 3.6 kHz. Adopting an OFDM modulation with a cyclic prefix length of $N_{\rm cp}T = 150$ ms and a symbol duration of $NT = 1.2$ s, we could pack 4320 carriers into the available bandwidth of 3.6 kHz. However, as explained, such a large number of carriers leads to a considerable receiver cost. Hence, we have split the band into $J = 16$ subbands of $K = 256$ carriers each, with $G = 14$ guard carriers in between the subbands ($G/2 = 7$ "guard" carriers are placed before the first and after the last subband). The guard bands allow for a Doppler spread of $G/(NT) = 14/1.2 \approx 12$ Hz between the OFDM subbands, which is much more than the Doppler spread that was encountered at sea. The timing offsets are chosen as $N_j T = j2$ ms, and the subband carrier frequencies f_j are offset from the overall center frequency $f_{\rm c}$ according to $f_j = f_{\rm c} + (j-7.5)(K+G)/(NT) = f_{\rm c} + (j-7.5) \times 225$ Hz. Note that we do not detail the exact value of the rate $1/T$, since it has a negligible influence on the performance as long as it is larger than the signal bandwidth.

Every OFDM symbol contains $K_{\rm t} = 160$ pilots per data vector $\mathbf{s}_p$ divided into $M = 32$ pilot clusters of length $K_{\rm t}/M = 5$. Hence, the number of data symbols per data vector is $K_{\rm d} = K - K_{\rm t} = 96$. Every cluster is designed according to [17], which is a generalization of the cluster design proposed in [18]. Basically, we put a single nonzero pilot in the middle and surround it by zeros. To improve the efficiency at low SNR, the available power is equally distributed among data symbols and pilots, as indicated in [18]. Since the overall energy of $\mathbf{s}_p$ is set to K, the nonzero pilots have an energy $K/(2M) = 4$, versus an energy $K/(2K_{\rm d}) = 4/3$ for the data carriers.

To end up in a covert working regime, we employ a turbo code of rate $1/3$ and we also spread the data vectors $\mathbf{s}_p$ over a total of I OFDM time slots and $J = 16$ subbands using a QPSK constellation. We consider two different modulation schemes, a low data rate (LDR) and a high data rate (HDR) scheme. In the LDR scheme, we employ a rate-1/3 turbo code encoding 125 information bits into 192 QPSK data symbols, covering $P = 2$ data vectors. These are then spread over $I = 21$ OFDM time slots, leading to a data rate of $125/(21 \times 1.35) \approx 4.4$ bit/s. In the HDR scheme, a different rate-1/3 turbo code is adopted, which encodes 637 information bits into 960 QPSK symbols, covering 10 data vectors. Three of such code blocks, i.e., $P = 30$ data vectors, are grouped and spread over $I = 17$ OFDM time slots, leading to a data rate of $1911/(17 \times 1.35) \approx 83$ bit/s. The effective data rates are 4.2 and 78 bit/s if the overhead of the preamble is taken into account.

Three cases are considered with various delay and Doppler spreads. Fig. 5 shows typical power delay profiles and Doppler spectra. Cases A and B correspond to the sea trials carried out in the Baltic Sea. An acoustic modem with a carrier frequency of $f_{\rm c} = 3.3$ kHz was suspended in the water column at a depth of about 40 m. It was deployed from a surface ship that used dynamic positioning to stay at a fixed position. On the other side of the link, a vertical hydrophone chain was deployed from an anchored ship. Only a single hydrophone at a depth of 50 m was used for the analysis. From Fig. 5 we observe a crescendo of multipath arrivals with a delay spread that increases with range. Two ranges are shown, 8 km (Case A) and 52 km (Case B). These cases only reveal a small Doppler spread, because they correspond to the situation where the ships have little motion and the signals are trapped in a sound channel with no surface interaction [19], [20]. For Cases A and B, successive cycles were broadcast where in each cycle the source level was reduced by 2 dB. The results are shown in Figs. 6 and 7, respectively, where a cross indicates a detection failure. The signal-to-noise ratio (SNR) of the recorded signals is computed as discussed in [20] with an uncertainty of about 2 dB. Owing to the small Doppler spread, it is better to use the time-invariant channel estimator here ($Q = 1$). The HDR signals are correctly decoded down to an SNR of -9 dB and -8 dB for Cases A and B, respectively. For the LDR signals, the last error free cycle is below -16 dB for Case A and it is at -14 dB for Case B. The delay spread thus appears to have some negative influence on the performance, although it is not severe.

Case C is taken from an experiment on the Norwegian continental shelf. Another transducer with a carrier frequency of $f_{\rm c} = 5$ kHz was used, which broadcast the OFDM waveforms at an interval of eight minutes. During the experiment, the transmitter ship towed the modem at a nominal depth of 60 m and a nominal speed of 2.5 m/s, starting nearby and reaching a distance of 38 km. A receive hydrophone at a depth of 90 m was selected for this experiment. From 5, we clearly see a different delay profile compared to Cases A and B. Moreover, the Doppler spectrum has broadened, partly because wave motion is transferred onto the transmitter, and partly because the Norwegian coastal communication channel is more dynamic than the sound channel in the Baltic Sea. Surface interactions are not excluded. Here, it turns out that the time-varying channel estimator does better than the time-invariant one (not shown). Fig. 8 shows the decoding results, with successful HDR decoding down to an SNR of -5 dB and successful LDR decoding down to an SNR below -14 dB. At a range of $\approx$20 km there are loud crunch and click sounds, produced somewhere on the receiver ship, which cause a dip in the SNR and an isolated HDR failure.

In all analyzed at-sea experiments, many more than shown in the present paper, receiver diagnostics reveal that the SNR limit for LDR is reached because of detection failures, or is not reached because the experiment did not go down far enough in SNR to cause detection or demodulation failures. Hence, for LDR, the limits of the OFDM scheme are not yet reached.

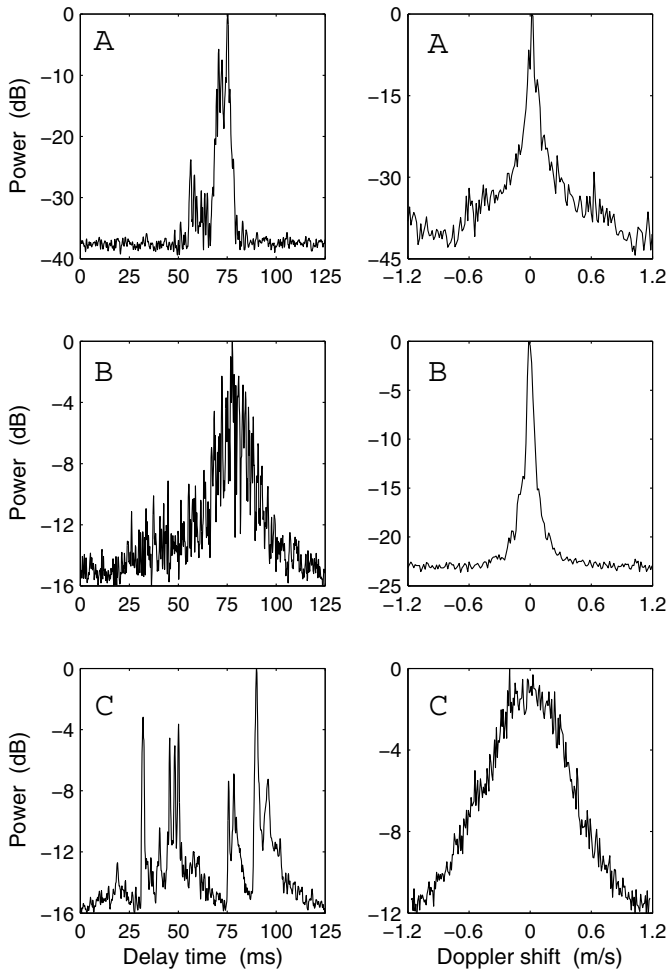

Fig. 5. Delay profiles and Doppler spectra (after removal of the mean Doppler shift) for the different case studies.

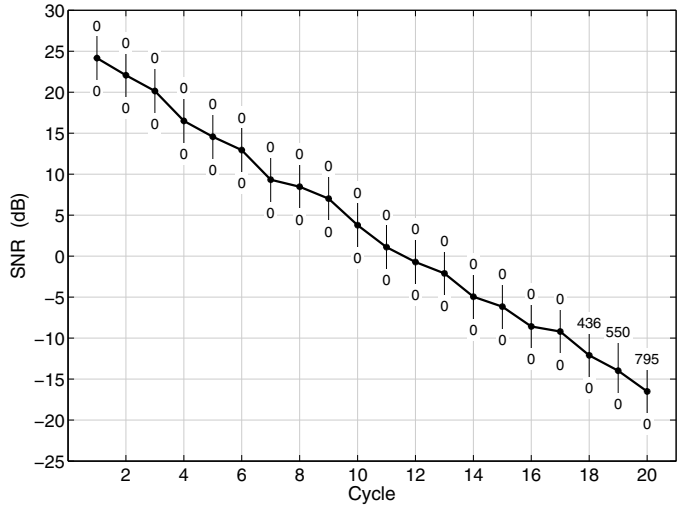

Fig. 6. SNR and BER results for LDR and HDR, respectively plotted below and above the curve (Case A, $L_\lambda = 8$, $Q = 1$).

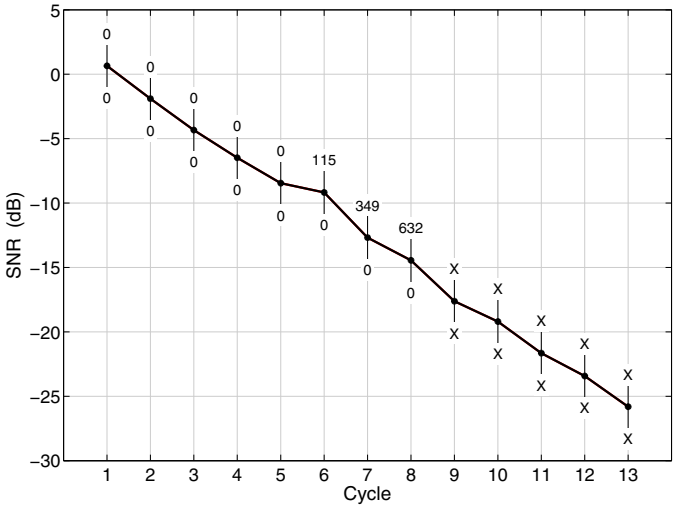

Fig. 7. SNR and BER results for LDR and HDR, respectively plotted below and above the curve (Case B, $L_\lambda = 8$, $Q = 1$).

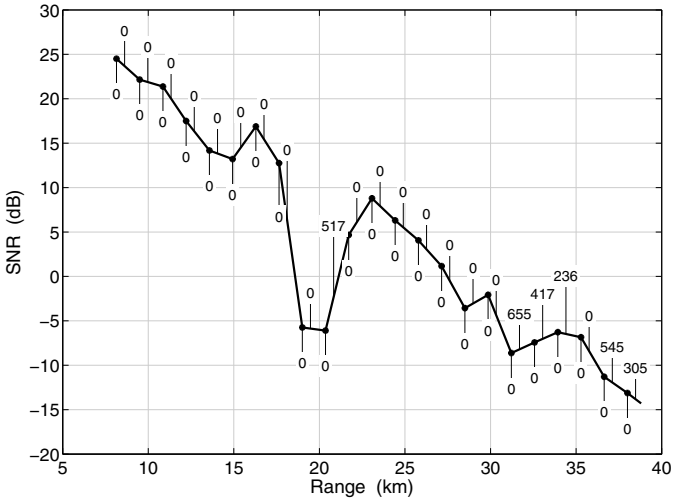

Fig. 8. SNR and BER results for LDR and HDR, respectively plotted below and above the curve (Case C, $L_\lambda = 8$, $Q = 3$).

VI. Conclusions

A multiband OFDM modulation is presented for covert underwater communications. Compared with a single-band OFDM system, the multiband approach with joint equalization and despreading leads to a significant reduction of the receiver complexity. The demodulation time from raw data to user bits amounts to 8–13 s, depending on the choice between the time-invariant and time-variant channel estimator, and the data rate, in a Matlab implementation running on an Intel® Core$^{\mathrm{TM}}$2 Duo Desktop Processor E6420. The algorithms were tested during sea trials in littoral waters under different conditions. The results reveal that a data rate of 78 bit/s could be successfully demodulated at a low SNR, the value of which depends on the circumstances. At 4.2 bit/s, system performance is not limited by the OFDM scheme, but by detection and initial

synchronization. Detection is in fact an open problem for noiselike, Doppler-sensitive preambles. The proposed OFDM system has been implemented in prototype acoustic modems, which will be tested between a UUV and a mother ship during sea trials in 2008.

ACKNOWLEDGMENT

This work was performed under the EUROPA MOU ERG No1, RTP 110.060 "UUV Covert Acoustic Communications". The Dutch contribution was sponsored by the Defence Research and Development Department of the Netherlands Ministry of Defence. Geert Leus is supported in part by NWO-STW under the VIDI program (DTC.6577).

REFERENCES

[1] T. C. Yang and W.-B. Yang, "Performance analysis of direct-sequence spread-spectrum underwater acoustic communications with low signal-to-noise-ratio input signals," *Journal of the Acoustical Society of America*, vol. 123, no. 2, pp. 842–855, February 2008.

[2] E. Sangfelt, B. Nilsson, and J. Israelsson, "Covert underwater communication experiments using DSSS and turbo equalization," in *UDT Europe 2008*, Glasgow, United Kingdom, June 2008.

[3] S. Coatelan and A. Glavieux, "Design and test of a multicarrier transmission system on the shallow water acoustic channel," in *OCEANS 1994*, Brest, France, September 1994, pp. III/472–III/477.

[4] M. Stojanovic, "Low complexity OFDM detector for underwater acoustic channels," in *OCEANS 2006*, Boston, Massachusetts, USA, September 2006.

[5] B. Li, S. Zhou, M. Stojanovic, L. Freitag, and P. Willet, "Non-uniform Doppler compensation for zero-padded OFDM over fast-varying underwater acoustic channels," in *OCEANS 2007*, Vancouver, Canada, 2007.

[6] M. K. Tsatsanis and G. B. Giannakis, "Modeling and equalization of rapidly fading channels," *International Journal of Adaptive Control and Signal Processing*, vol. 10, no. 2/3, pp. 159–176, March 1996.

[7] Z. Tang, R. C. Cannizzaro, G. Leus, and P. Banelli, "Pilot-assisted time-varying channel estimation for OFDM systems," *IEEE Transactions on Signal Processing*, vol. 55, no. 5, pp. 2226–2238, May 2007.

[8] W. G. Jeon, K. H. Chang, and Y. S. Cho, "An equalization technique for orthogonal frequency-division multiplexing systems in time-variant multipath channels," *IEEE Transactions on Communications*, vol. 47, no. 1, pp. 27–32, January 1999.

[9] P. Schniter, "Low-complexity equalization of OFDM in doubly-selective channels," *IEEE Transactions on Signal Processing*, vol. 52, no. 4, pp. 1002–1011, April 2004.

[10] L. Rugini, P. Banelli, and G. Leus, "Simple equalization of time-varying channels for OFDM," *IEEE Communications Letters*, vol. 9, no. 7, pp. 619–621, July 2005.

[11] L. Rugini, P. Banelli, and G. Leus, "Low-complexity banded equalizers for OFDM systems in doppler spread channels," *EURASIP Journal on Applied Signal Processing*, vol. 2006, pp. Article ID 67404, 13 pages, 2006.

[12] C. Heegard and S. B. Wicker, *Turbo Coding*, Springer, 1998.

[13] M. Tüchler, A. C. Singer, and R. Koetter, "Minimum mean squared error equalization using a priori information," *IEEE Transactions on Signal Processing*, vol. 50, no. 3, pp. 673–683, March 2002.

[14] R. Otnes and M. Tüchler, "Iterative channel estimation for turbo equalization of time-varying frequency-selective channels," *IEEE Transactions on Wireless Communications*, vol. 3, no. 6, pp. 1918–1923, November 2004.

[15] K. Fang and G. Leus, "Low-complexity block turbo equalization for OFDM systems in time-varying channels," in *Proc. of the IEEE International Conference on Acoustics, Speech, and Signal Processing (ICASSP)*, Honolulu, Hawaii, April 2007, pp. III/445–III/448.

[16] K. Fang, L. Rugini, and G. Leus, "Iterative channel estimation and turbo equalization for time-varying ofdm systems," in *Proc. of the IEEE International Conference on Acoustics, Speech, and Signal Processing (ICASSP 2008)*, Las Vegas, Nevada, USA, March/April 2008, To appear.

[17] A. P. Kannu and P. Schniter, "MSE-optimal training for linear time-varying channels," in *Proc. of the IEEE International Conference on Acoustics, Speech, and Signal Processing (ICASSP)*, Philadelphia, Pennsylvania, March 2005, pp. III/789–III/792.

[18] X. Ma, G. B. Giannakis, and S. Ohno, "Optimal training for block transmissions over doubly-selective fading channels," *IEEE Transactions on Signal Processing*, vol. 51, no. 5, pp. 1351–1366, May 2003.

[19] H. S. Dol, F. Gerdes, P. A. van Walree, W. Jans, and S. Künzel, "Acoustic channel characterization in the Baltic Sea and in the North Sea," in *OCEANS 2008*, Quebec City, Canada, September 2008.

[20] P. van Walree, E. Sangfelt, and G. Leus, "Multicarrier spread spectrum for covert acoustic communications," in *OCEANS 2008*, Quebec City, Canada, September 2008.